



Supplement of

Understanding high wintertime ozone pollution events in an oil and natural gas producing region of the western US

R. Ahmadov et al.

Correspondence to: R. Ahmadov (ravan.ahmadov@noaa.gov)

1 **Understanding high wintertime ozone pollution events in an**
2 **oil and natural gas producing region of the western U.S.**

3 ***Supplemental Information***

4 **1 Regression Slopes in the Top-Down Inventory**

5 Details of the measurements of NO_y and the various VOCs during the winters of 2012 and 2013
6 at the Horse Pool site are presented in Edwards et al. (2013) and the report available at:
7 <http://www.deq.utah.gov/locations/U/uintahbasin/studies/UBOS-2013.htm>. Most VOC species
8 were determined by GC-MS in 2012, and GC-FID in 2013 as in Gilman et al. (2013). Aromatics
9 and formaldehyde were determined by PTR-MS in both years (de Gouw and Warneke,
10 2007;Warneke et al., 2011). During 2012 one-minute average NO_y data were determined by
11 catalytic conversion of NO_y over heated gold and chemiluminescence detection of NO (Williams
12 et al., 2009), and in 2013 it was determined by molybdenum conversion and cavity ringdown
13 detection of NO₂ as described in Wild et al., (2014). One minute average CH₄ was determined
14 using a 3-channel Picarro instrument (Peischl et al., 2012).

15 Linear regressions of NO_y and VOCs with CH₄ are windowed between the hours of 1000 and
16 1600 MST to capture regionally representative conditions within the daytime boundary layers
17 and minimize effects from isolated plumes observed under more stable conditions. Half-hourly
18 resolution VOCs data from both years are included in the regressions. Table S1 summarizes the
19 linear regressions and slopes with respect to CH₄. VOC emissions are dominated by light alkanes
20 on a molar basis with higher correlations ($r^2 > 0.85$) for primary VOCs, and lower correlations
21 for secondary, oxygenated VOCs. The table also gives the recommended assignment of each
22 VOC into the Statewide Air Pollution Research Center (SAPRC-07) photochemical mechanism
23 (Carter, 2010) or the RACM mechanism (Stockwell et al., 1997), which is a basis for the
24 mechanism used in this study. The same lumped hydrocarbon and oxygenated VOC species are
25 emitted in both emission scenarios.

26 **2 Comparison of the meteorological simulations**

27 Figure S2a-c shows averaged diurnal time series for meteorological variables – temperature,
28 moisture, wind speed and direction measured at Horse Pool during the evaluation time period

29 January 29 – February 8, 2013. The wind speed and direction are reasonably well simulated
30 during the daytime. However, at nights the model shows stronger easterly winds, whereas the
31 observations indicate lighter winds from east and south-east. The comparisons also show that
32 WRF captures the cold pool conditions with ~2 °C bias during daytime at Horse Pool (Figure
33 S2a). The model shows a stronger katabatic flow at night, which could be due to the cold bias in
34 the model in the evening hours (Figures S2a,c).

35 We also compared PBL height estimates from the model and the observations in order to assess
36 the model's ability to simulate the cold pool and vertical mixing. Using tethersonde
37 measurements of temperature and relative humidity at 3 locations conducted by the NOAA
38 Global Monitoring Division between January 29 and February 8, 2013, PBL heights were
39 estimated from the vertical gradient of virtual potential temperature. The same method was
40 applied to the model output at corresponding times and locations. The results are shown in
41 Figure S3. The majority of the daytime (0900-1700 MST) PBL height values fall within the
42 range of 50-200 m, with a median of all the measurements of 110 m. Although the model
43 simulates the observed range of the mixed layer depth, it has difficulty in capturing the timing of
44 growth and collapse of the PBL observed within the UB (Figure S3).

45

46

47

48

49

50

51

52

53

54

55

56 Table S1. Linear regression slope (ppbv/ppmv), standard deviation of fit (StDv (ppbv/ppmv)), r^2
 57 correlation coefficient, VOC species assignments to the SAPRC-07 and RACM chemical
 58 mechanisms for 1000–1600 MST observations at Horse Pool during the winters of 2012 and
 59 2013.

VOC	Slope	StDv	r^2	SAPRC-07 VOC assignment	RACM VOC assignment
NO _y	3.026	0.56	0.65	-	-
Ethane	57.87	1.02	0.96	ALK1	ETH
Propane	26.47	0.38	0.97	ALK2	0.519*HC3
Methanol	9.152	1.67	0.34	MEOH	0.402*HC3
n-butane	8.902	0.23	0.94	ALK3	1.11*HC3
i-butane	5.861	0.16	0.94	ALK3	1.11*HC3
i-pentane	3.897	0.11	0.94	ALK4	0.964*HC5
n-pentane	3.532	0.17	0.90	ALK4	0.964*HC5
2 and 3 methylpentane	2.942	0.21	0.86	ALK4	HC5
1-methyl cyclohexane	2.091	0.03	0.96	ALK5	HC8
n-hexane	1.613	0.06	0.92	ALK4	0.17*HC5+0.83*HC8
Acetone	1.541	0.25	0.71	ACET	0.253*KET
Cyclohexane	1.178	0.01	0.97	ALK5	HC8
1-methyl cyclopentane	0.966	0.02	0.95	ALK4	0.956*HC5
2,2 dimethylbutane	0.863	0.68	0.11	ALK3	0.964*HC3
Acetaldehyde	0.861	0.11	0.75	CCHO	ALD
n-heptane	0.807	0.06	0.86	ALK4	HC5
Toluene	0.758	0.03	0.90	ARO1	TOL
Formaldehyde	0.638	0.06	0.80	HCHO	HCHO
Benzene	0.593	0.00	0.97	0.295*ARO1	0.293*TOL
MEK	0.568	0.09	0.72	MEK	KET
n-octane	0.548	0.02	0.92	ALK5	0.945*HC8
1,3 dimethylcyclohexane	0.386	0.01	0.94	ALK5	HC8
Ethylene	0.353	0.02	0.85	ETHE	OL2
C8 aromatics	0.349	0.02	0.85	ARO2	XYL
n-nonane	0.216	0.01	0.87	ALK5	HC8
Ethanol	0.161	0.09	0.26	ALK3	1.198*HC3
Acetylene	0.146	0.06	0.41	ALK2	0.343*HC3
1,1,3	0.086	0.01	0.71	ALK5	HC8
2,2 dimethylpropane	0.085	0.02	0.56	ALK2	0.44*HC3
1,2 dimethylcyclohexane	0.078	0.00	0.94	ALK5	HC8
n-decane	0.075	0.00	0.85	ALK5	HC8
C9 aromatics	0.071	0.01	0.75	.0879*ARO1+.9121*A	.0879*TOL+.9121XY
2,2 dimethylbutane	0.059	0.00	0.91	ALK3	0.964*HC8
Propanal	0.057	0.01	0.59	RCHO	ALD
Ethylbenzene	0.051	0.00	0.92	ARO1	TOL

Ethylcyclohexane	0.049	0.00	0.92	ALK5	HC8
n-undecane	0.046	0.00	0.82	ALK5	HC8
1,3 dimethylcyclohexane	0.043	0.00	0.93	ALK5	HC8
1,2,4 trimethylbenzene	0.040	0.00	0.87	ARO2	XYL
Furan	0.035	0.03	0.00	ARO2	XYL
1,3,5 trimethylbenzene	0.030	0.00	0.86	ARO2	XYL
Naphthalene	0.030	0.00	0.59	ARO2	XYL
Propylene	0.028	0.00	0.71	OLE1	OLT
1-eth,3,4-methylbenzene	0.023	0.00	0.89	ARO2	XYL
C10 aromatics	0.014	0.00	0.78	.061*ARO1+.939*ARO	.061*TOL+.939*XY
Hexanal	0.013	0.00	0.33	RCHO	ALD
1,2,3 trimethylbenzene	0.012	0.00	0.81	ARO2	XYL
Butanal	0.009	0.00	0.51	RCHO	ALD
n-propylbenzene	0.007	0.00	0.88	ARO1	TOL
C11 aromatics	0.006	0.00	0.61	.0246*ARO1+.975*AR	.0246*TOL+.939*XY
i-propylbenzene	0.005	0.00	0.90	ARO1	TOL
1-eth,2-methylbenzene	0.005	0.00	0.88	ARO2	XYL
Benzaldehyde	0.004	0.00	0.71	BALD	ALD
Methacrolein	0.004	0.00	0.48	MACR	MACR
MVK	0.004	0.00	0.73	MVK	0.5*KET+0.5*OLT
C12 aromatics	0.003	0.00	0.47	ARO2	XYL
1,3 butadiene	0.002	0.00	0.60	OLE2	OLI
Vinylbenzene	0.002	0.00	0.19	OLE2	TOL
Isoprene	0.000	0.02	0.00	ISOP	ISO

60

61

62

63

64

65

66

67 Table S2. WRF-Chem model configuration. Full description of the model options can be found
68 in: www.wrf-model.org and <http://ruc.noaa.gov/wrf/WG11/>.

Horizontal resolution	12 and 4 km nested domains
Vertical resolution	60 layers (18 within lowest 500 m)
Meteorological input	NAM analysis
Surface layer	MYNN
Planetary boundary layer	MYNN level 2.5
Land Surface	Noah Land Surface Model
Microphysics	WRF Single-Moment 5-class
Shortwave and longwave radiation	RRTMG
Gas-phase chemistry	RACM_ESRL
Transport of species	advection and vertical mixing
Advection option for chemical variables	Monotonic

69

70

71

72

73

74

75

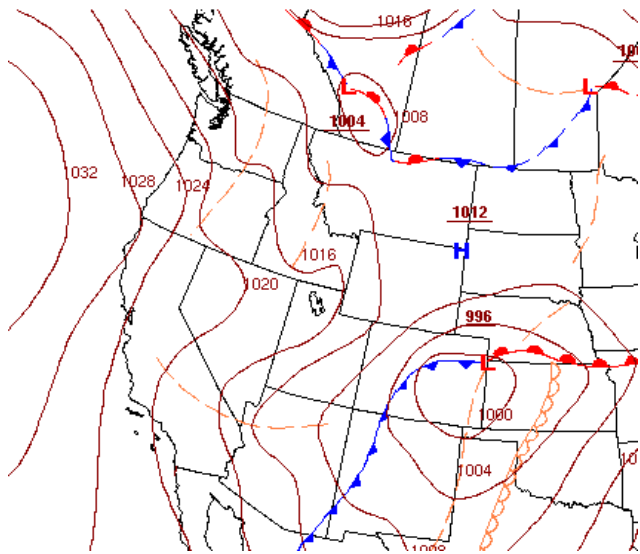
76

77

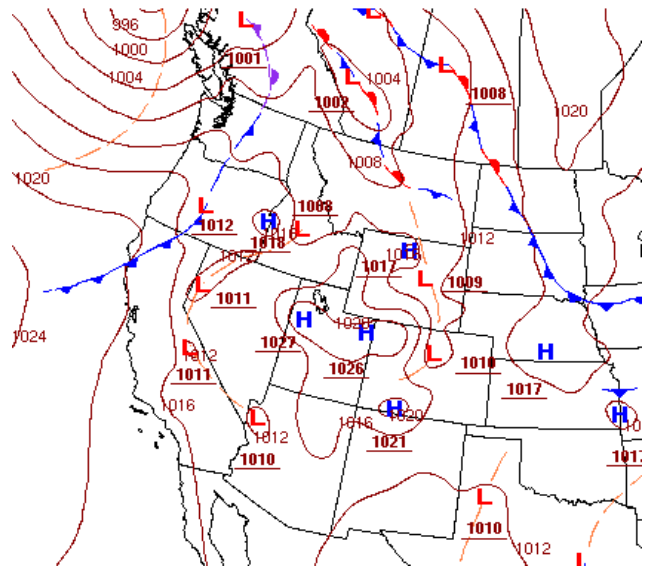
78

79 Figure S1. Weather maps from NOAA/HPC (<http://www.hpc.ncep.noaa.gov>); a) frontal passage,
80 1400 MST, January 28, 2013; b) stagnation episode, 1400 MST, February 5, 2013;

81 a)



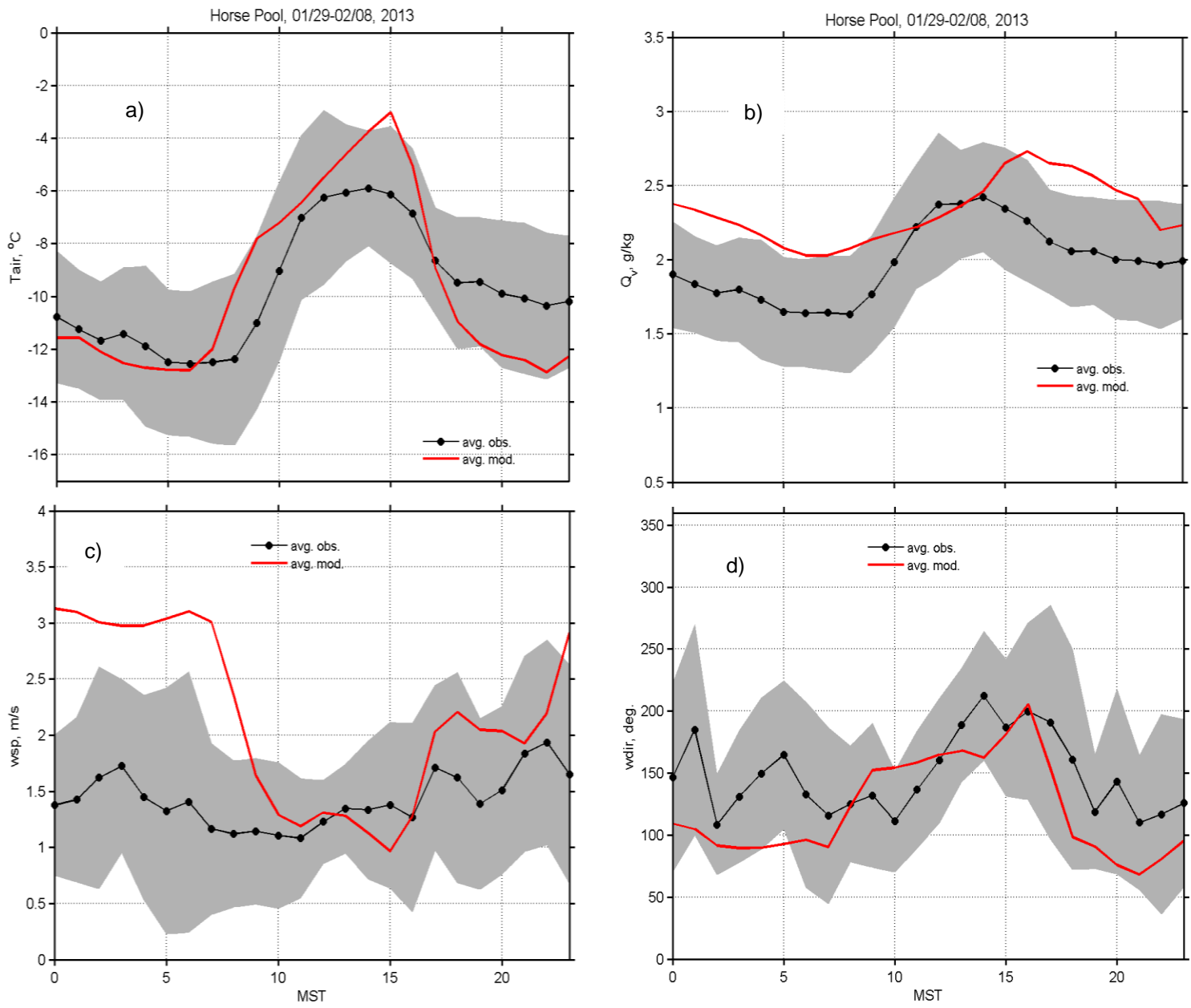
b)



82

83 Figure S2. Averaged diurnal cycle of meteorological variables (modeled and measured) during
84 January 29 – February 8, 2013. The shaded area on the plots depict the $\pm\sigma$ (standard deviation)
85 of the observed values; a) Air temperature, b) water vapor mixing ratio, c) wind speed and d)
86 wind direction

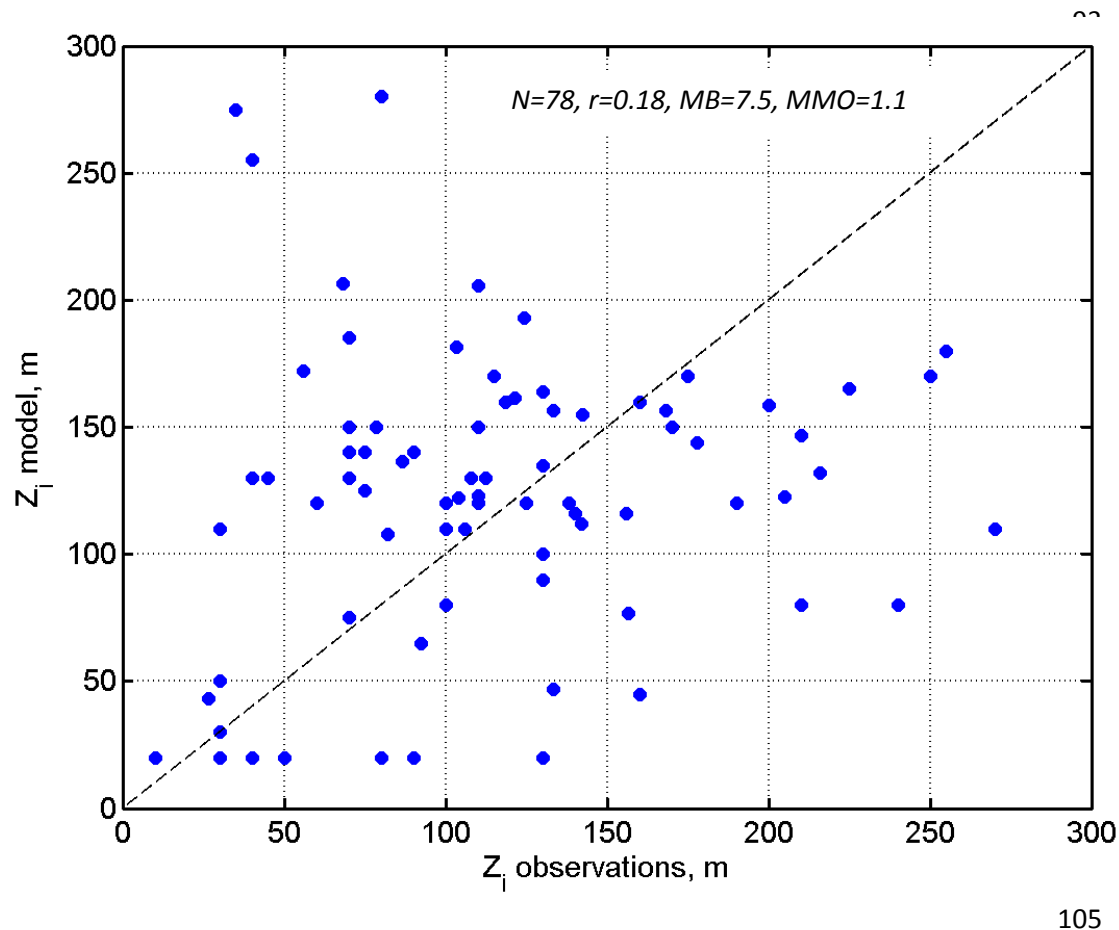
87



88

89

90 Figure S3. Mixing layer height estimates (3 hourly averaged) determined from vertical profiles
91 of virtual potential temperature from the model output and tethersonde measurements during
92 daytime (0900 -1700 MST), January 29 – February 8, 2013.



106

107

108

109

110

111

112

113 **References**

- 114 Carter, W. P. L.: Development of the SAPRC-07 chemical mechanism, *Atmos. Environ.*, 44,
115 5324-5335, 10.1016/j.atmosenv.2010.01.026, 2010.
- 116 de Gouw, J., and Warneke, C.: Measurements of volatile organic compounds in the earth's
117 atmosphere using proton-transfer-reaction mass spectrometry, *Mass Spectrometry Reviews*, 26,
118 223-257, doi:210.1002/mas.20119, 2007.
- 119 Edwards, P. M., Young, C. J., Aikin, K., deGouw, J., Dube, W. P., Geiger, F., Gilman, J.,
120 Helmg, D., Holloway, J. S., Kercher, J., Lerner, B., Martin, R., McLaren, R., Parrish, D. D.,
121 Peischl, J., Roberts, J. M., Ryerson, T. B., Thornton, J., Warneke, C., Williams, E. J., and Brown,
122 S. S.: Ozone photochemistry in an oil and natural gas extraction region during winter:
123 simulations of a snow-free season in the Uintah Basin, Utah, *Atmos. Chem. Phys.*, 13, 8955-
124 8971, 10.5194/acp-13-8955-2013, 2013.
- 125 Gilman, J. B., Lerner, B. M., Kuster, W. C., and de Gouw, J. A.: Source Signature of Volatile
126 Organic Compounds from Oil and Natural Gas Operations in Northeastern Colorado, *Environ.*
127 *Sci. Technol.*, 47, 1297-1305, 10.1021/es304119a, 2013.
- 128 Peischl, J., Ryerson, T. B., Holloway, J. S., Trainer, M., Andrews, A. E., Atlas, E. L., Blake, D.
129 R., Daube, B. C., Dlugokencky, E. J., Fischer, M. L., Goldstein, A. H., Guha, A., Karl, T.,
130 Kofler, J., Kosciuch, E., Misztal, P. K., Perring, A. E., Pollack, I. B., Santoni, G. W., Schwarz, J.
131 P., Spackman, J. R., Wofsy, S. C., and Parrish, D. D.: Airborne observations of methane
132 emissions from rice cultivation in the Sacramento Valley of California, *J. Geophys. Res.-Atmos.*,
133 117, 10.1029/2012jd017994, 2012.
- 134 Stockwell, W. R., Kirchner, F., Kuhn, M., and Seefeld, S.: A new mechanism for regional
135 atmospheric chemistry modeling, *J. Geophys. Res.-Atmos.*, 102, 25847-25879, 1997.
- 136 Warneke, C., Veres, P., Holloway, J. S., Stutz, J., Tsai, C., Alvarez, S., Rappenglueck, B.,
137 Fehsenfeld, F. C., Graus, M., Gilman, J. B., and de Gouw, J. A.: Airborne formaldehyde
138 measurements using PTR-MS: calibration, humidity dependence, inter-comparison and initial
139 results, *Atmos. Meas. Tech.*, 4, 2345-2358, 10.5194/amt-4-2345-2011, 2011.
- 140 Wild, R., Edwards, P., Dube, W., Baumann, K., Edgerton, E., Quinn, P., Roberts, J., Rollins, A.,
141 Veres, P., Warneke, C., Williams, E., Yuan, B., Brown, S.: A Measurement of Total Reactive
142 Nitrogen, NO_y, together with NO₂, NO, and O₃ via Cavity Ring-down Spectroscopy, (*accepted*)
143 ES&T, 2014.

144 Williams, E. J., Lerner, B. M., Murphy, P. C., Herndon, S. C., and Zahniser, M. S.: Emissions of
145 NO_x, SO₂, CO, and HCHO from commercial marine shipping during Texas Air Quality Study
146 (TexAQS) 2006, *J. Geophys. Res.-Atmos.*, 114, 10.1029/2009jd012094, 2009.